Temperature-Dependent Conformational Transitions and Hydrogen-Bond Dynamics of the Elastin-Like Octapeptide GVG(VPGVG): A Molecular-Dynamics Study

Roger Rousseau,*† Eduard Schreiner,* Axel Kohlmeyer,* and Dominik Marx*
*Lehrstuhl für Theoretische Chemie, Ruhr-Universität Bochum, Bochum, Germany and †International School for Advanced Studies, Trieste, Italy

ABSTRACT A joint experimental/theoretical investigation of the elastin-like octapeptide GVG(VPGVG) was carried out. In this article a comprehensive molecular-dynamics study of the temperature-dependent folding and unfolding of the octapeptide is presented. The current study, as well as its experimental counterpart (see companion article in this issue) find that this peptide undergoes an inverse temperature transition (ITT), leading to a folding at ~40–60°C. In addition, an unfolding transition is identified at unusually high temperatures approaching the normal boiling point of water. Due to the small size of the system, two broad temperature regimes are found: the ITT regime at ~10–60°C and the unfolding regime at $\sim T >$ 60°C, where the peptide has a maximum probability of being folded at $T \approx$ 60°C. A detailed molecular picture involving a thermodynamic order parameter, or reaction coordinate, for this process is presented along with a time-correlation function analysis of the hydrogen-bond dynamics within the peptide as well as between the peptide and solvating water molecules. Correlation with experimental evidence and ramifications on the properties of elastin are discussed.

INTRODUCTION

Vertebrate elastic fibers, as contained in vascular walls, skin, or lungs, allow for reversible deformations upon mechanical stress. These fibers consist of two main types of protein components: a fibrous component, fibrilen; and an amorphous component, the globular elastin protein (Pasquali-Ronchetti et al., 1995). The essential elasticity is provided by the latter protein, elastin, which is known to have very unique viscoelastic properties in the water-swollen state; see Debelle and Alix (1999), Debelle and Tamburro (1999), Martino et al. (2002), Reiersen and Rees (2001), Urry (1997), and Urry et al. (2002) for recent overviews. The insoluble elastin is an extensively cross-linked polymer of a precursor tropoelastin. Tropoelastin is composed of two types of domains. One of them is rich in lysine and provides cross-linking of the individual monomers resulting in lysinonorleucin, desmosine, and isodesmosine links, which are responsible for its typical yellow color. The other is made predominantly of hydrophobic amino acids with the highly repetitive pentameric repeat unit, VPGVG (amino acids valine, *V*; proline, *P*; and glycine, *G*) which has been found to be crucial to elastin's functionality (Reiersen et al., 1998; Urry, 1993, 1997; Urry et al., 2002).

An interesting peculiarity of both elastin and tropoelastin, is that they undergo folding by increasing the temperature beyond typically 25°C. The term *inverse temperature transition* (ITT) was coined for this apparently paradoxical change from a disordered (extended) to an ordered (folded) conformation upon heating. A striking manifestation of this phenomena is the ability to grow crystalline solid-state structures from a solution of cyclic elastin-like oligopeptides by heating (Cook et al., 1980; Urry et al., 1978). As such, tropoelastin and its synthetic analogs have been a subject of intense investigation in the field of biopolymers and protein engineering. Elastin-like polymers have the promise of providing materials for biomechanical devices (Nath and Chilkoti, 2001; Urry, 1993, 1997) as well as temperature-dependent molecular switches (Reiersen et al., 1998). Despite the intense research efforts, the detailed structure of tropoelastin still defeats elucidation. Hence a molecular-level picture which relates the protein structure to the viscoelastic properties is still a matter of debate. What is beyond doubt, however, is the decisive role of water as a plasticizer; dry elastin is brittle (Partridge, 1962). Still, the potentially crucial aspect of the protein's hydration water remains largely unexplored with the notable exception of recent molecular-dynamics (MD) simulations (Li et al., 2001b).

The origin of the viscoelastic properties of elastin is controversially discussed, recalling concepts such as classical rubber elasticity (Hoeve and Flory, 1974), various librational entropy mechanism (Debelle and Tamburro, 1999; Urry, 1993; Wasserman and Salemme, 1990), and multiphase models (Debelle and Alix, 1999; Li et al., 2001b). Much of the experimental data has been summarized in excellent reviews (Li and Daggett, 2002; Martino et al., 2002; Urry, 1997) on both elastin and elastin-like polypeptides. Much data exist that suggest that both elastin and its synthetic mimics display an interesting conformational dynamics in solution. Early nuclear magnetic resonance studies suggest that elastin under physiological conditions is composed of highly mobile chains (Fleming et al., 1980; Torchia and Piez, 1973), which correlated well with the observation from bi-

Submitted September 29, 2003, and accepted for publication December 12, 2003.

Address reprint requests to Eduard Schreiner, Lehrstuhl für Theoretische Chemie, Ruhr-Universität Bochum, Universitätsstraße 150, 44801 Bochum, Germany. Tel.: 49-234-322-2121; E-mail: eduard.schreiner@theochem.ruhr-uni-bochum.de.

0006-3495/04/03/1393/15 $2.00

refringence (Aaron and Gosline, 1980) measurements that elastin, in the same state, is isotropically distributed with the chains adopting random conformations. Studies of the thermomechanical properties of water-swollen elastin and tropoelastin are consistent with the interpretation of elastin as a classical rubber with heavy emphasis on the role of entropic contributions to elasticity (Hoeve and Flory, 1974). These findings would support a single-phase model where the structure of elastin is random and undergoes large amplitude fluctuations. Recent single-molecule atomic force microscopy and spectroscopic measurements (Urry et al., 2002) studies have severely challenged this interpretation and suggest that, above the ITT temperature, a structurally ordered model of poly(VPGVG) can also account for these elastic properties due to significant protein librational contributions to the overall entropy as suggested two decades ago (Urry et al.,1983). Other spectroscopic experiments such as Fourier transform infrared (FT-IR), nuclear magnetic resonance (NMR), circular dichroism (CD), and Raman measurements (Debelle et al., 1995; Nicolini et al., 2004; Arad, 1990; Reiersen et al., 1998; E. Schreiner, C. Nicolini, B. Ludolph, R. Ravindra, N. Otte, A. Kohlmeyer, R. Rousseau, R. Winter, and D. Marx, unpublished material; Urry et al., 1985a) on elastin-like polypeptides suggest the presence of β- and γ-turns as a common structural motif which may be in dynamic equilibrium and very short and/or distorted antiparallel β-strands and disordered structures with possible dynamic sheet-coil-turn transitions. Recent NMR studies also point to the high mobility of the elastin chains in the water-swollen elastins (Perry et al., 2002); and in solution, multiple temperature states for poly(GVGVP), each with different dynamical behavior and peptide-water interactions, were observed (Kurková et al., 2003). These later data would instead support a multiphase model of elastin (Debelle and Alix, 1999), where the fine details of the protein structure and, in particular, its interactions with water, play a crucial role in understanding its elasticity. Overall, there is a wealth of data on the structure and properties of these systems, and although the models do not agree on their interpretation, a central ingredient is the intriguing and complex dynamical behavior of elastin-like polymers themselves and the crucial interplay with solvating water molecules.

Atomistic simulations on elastin or elastin-analogs are scarce. For early work, see Debelle and Tamburro (1999). Wasserman and Salemme (1990), in a review, studied the elastic properties of these proteins by performing short MD simulations under constraints to mimic an external pulling force. Here the authors found that entropic forces from reduced librational motion of the protein were indeed a main contributing factor in the elastic behavior. However, the authors were understandably limited to simulation times not exceeding 1 ns. It is noted that, in general, short simulation times generally lead to unreliable statistics, due to insufficient sampling of configuration space, and hence may provide only qualitative insights. A crucial factor also to be considered is the explicit atomistic treatment of the protein/water interface and characterization of its role in determining elastin's properties. As a significant advance along these lines, recent studies on solvated 90-amino-acid polypeptides of sequence $(VPGVG)_{18}$ have been reported, which explicitly include water (Li et al., 2001b). The importance of the protein/water interface was worked out based on thermodynamic and static structural—as opposed to dynamic—considerations. This work was successfully able to reproduce the ITT, clarifying how water may contribute to the entropic contribution to the elastic forces (Li et al., 2001a) as well as probe the role of elastin mimics as potential molecular machines (Li et al., 2002). Overall this work was successfully able to qualitatively relate its findings to much of the experimentally observed phenomena, although some debate has arisen with regard to the ability of the proposed structures to account for the temperature-dependence of elastin's water content above the ITT (Urry et al., 2002). Despite the significant improvement that these simulations have brought to our understanding of the atomic-level details concerning elastins' behavior, these quite-long biopolymers were simulated on the order of a few nanoseconds for a given temperature. In view of the expected long relaxation times of proteins of that size (Urry et al., 1985b), it would be highly desirable to have access to simulation times that allow for quantitative statistical-mechanical analysis for a given number of amino acids. This is especially true for low-frequency oscillations of the protein backbone, which play a central role in many models of elastin's properties. Furthermore, the dynamics and, in particular, the kinetics of hydrogen bonds, remains unexplored up to now. Thus, questions regarding the coupling of the dynamics of the protein, the protein/water interface, and hydrogen bonding remain open issues.

A significant experimental finding was the recent demonstration (Reiersen et al.,1998) that oligopeptides of the kind $GVG(VPGVG)_n$ display the ITT even in the limit of only one pentameric repeat unit. Using the limiting value $n = 1$ opens up the possibility to perform MD simulations that allow for fairly long simulation times with sufficiently many solvating water molecules. We therefore have launched a joint experimental/simulation study of the smallest possible elastin model, the octamer GVG(VPGVG) (having only $\approx$640 Da); see the companion article, Nicolini et al. (2004). This minimal elastin model was chosen, at the expense of experimental difficulties, to allow for extensive MD simulations, at 12 temperatures between 280 and 390 K, with a thorough conformational sampling of 32 ns each (after equilibration), followed by in-depth statistical mechanical analysis with a focus on dynamics. The current approach will allow us to obtain a crucial link between the multitude of experimental results and the atomistic simulations by directly comparing results obtained on essentially the same system under thermodynamically consistent conditions. Moreover, the detailed statistical mechanical analysis which is possible on the current MD simulations will provide a complementary

perspective on simulation work already existing in the literature.

METHODS, MODELS, AND TECHNICAL DETAILS

System

The system consists of an 8-amino-acid oligopeptide of sequence GVG(VPGVG) capped by methylamine ($-$NH-CH_3) and acetyl ($-$CO-CH_3) groups at its C- and N-termini, respectively. In accordance with the experimental finding (Reiersen et al., 1998) that VPGVG is the minimal repeat unit necessary for observing the ITT irrespective of the end groups, the caps are not expected to change the basic scenario as found in our complementary experimental study on the zwitterionic species (Nicolini et al., 2004; E. Schreiner, C. Nicolini, B. Ludolph, R. Ravindra, N. Otte, A. Kohlmeyer, R. Rousseau, R. Winter, and D. Marx, unpublished material; further checks are discussed below). The octapeptide is solvated with 2127 waters and its center of mass is fixed to the center of a 50 Å-diameter spherical droplet surrounded by stochastic boundary conditions (Brooks and Karplus, 1983). This sphere diameter allows us to maintain at least 3–4 molecules between the peptide and the stochastic boundary even for the configurations where elastin is at its maximum elongation of ~27 Å. We employ the all-atom CHARMM force field (MacKerell et al., 1998) for the peptide and the TIP3P (Jorgensen et al., 1983) water potential.

Simulations

Within the EGO molecular-dynamics package (Eichinger et al., 1997, 2000) a weak Berendsen thermostating scheme (coupling time constant of 100 fs) was used to control the temperature using a 1 fs MD time step and the SHAKE algorithm for fixing the bonds between hydrogen and heavy atoms. This conservative choice of parameters for a careful integration of the equations of motion has allowed us to perform stable simulations which included equilibration times of 2–5 ns (depending on temperature) before obtaining 32 ns trajectories at 12 temperatures between 280 and 390 K. An additional run was performed at 400 K (not shown) to stretch the temperature range as much as possible beyond the normal boiling point of water. For many properties, such as hydrogen-bond breaking and reformation-rate constants, the same trend as that obtained from extrapolation of the data from 340 to 390 K was observed. However, average structural parameters in particular showed deviations from this trend, which we interpret tentatively as failures of the simulation approach. Note that 400 K exceeds by ~100 K the temperature range for which the employed force fields for both water and the peptide are optimized, i.e., ambient conditions. As a convergence check, the run obtained at 280 K was extended to >40 ns to test the reliability of both average and dynamical properties of the protein; the results at 280 K are quoted for the 32 ns MD run for statistical consistency. Internal pressures inside the droplet were found to be <~0.1–0.2 kbar depending on the temperature, which is well below the pressure of the order-of-many-kbars required to suppress protein folding entirely (Nicolini et al., 2004; Tamura et al., 2000).

To cross-check the possible influence of the capping groups we have computed two 25 ns trajectories at 280 and 320 K in larger droplets (60 Å diameter with 3700 water molecules) for both the capped and zwitterionic peptides. We obtained qualitatively identical results to those presented here, indicating that the ITT is neither significantly affected by the presence of the caps (which is in line with experimental findings; see Reiersen et al., 1998), nor by the spherical boundary conditions for the chosen size of the solvating droplet.

Hydrogen-bond analysis

Concerning the definition of hydrogen bonds (HBs) in water, and thus the population variable, $h(t)$, we employ a standard structural criterion based on both the distance ($R_{OH} < 2.6$ Å as obtained from including the entire first nearest-neighbor peak in the intermolecular OH radial distribution function) and the angle, $\angle_{O-H\cdots O} > 130°$ for $h(t) = 1$ (Luzar, 2000; Luzar and Chandler, 1996a,b; Starr et al., 1999; Stillinger, 1975; Xu and Berne, 2001). As a check we also performed the analysis with only the distance criterion, and yet again with the distance criterion, but using a tighter angular criterion of $\angle_{O-H\cdots O} > 150°$. Consistent with previous findings (Starr et al., 1999; Xu and Berne, 2001) the absolute value of rate constants, k_w and $\tilde{k}_w$, is sensitive to the actual choice of the parameters of the definition and was found to vary as much as a factor of 2–3 between different definitions. However, we always obtained the same qualitative trends that both HB numbers and rate constants (k_w and $\tilde{k}_w$) feature a linear behavior with respect to temperature. Similarly, for peptide/peptide and peptide/water HBs, the same criterion based on distances ($R_{AH} < 2.6$ Å where the proton acceptor, A, is either an oxygen atom of a water molecule or of a peptide carbonyl group) and angles ($\angle_{D-H\cdots A} > 130°$ with the proton donor, D, being either a water O-atom or peptide backbone N-atom) was used. As a check we varied the distance to $R_{AH} < 2.4$ Å, keeping the angle cutoff unaltered, and performed the analysis with only the distance criterion. Again we found the same general behavior of two temperature regimes based on the dynamics of peptide/water HBs and the temperature-dependence of n_{pp} (*p*eptide-*p*eptide) and n_{bw} (*b*ridging *w*ater, i.e., peptide-water-peptide) to be preserved. In conclusion, although the HB definitions do change the reported absolute values of the HB numbers and rate constants as expected (Starr et al., 1999; Xu and Berne, 2001), the qualitative behavior remains the same, and thus the trends in the temperature-dependence for these quantities are not affected.

Principal component analysis

Principal component analysis (PCA) is a standard projection method in statistical data analysis, feature extraction, and data compression (Hyvärinen et al., 2001). It also turned out to be a very useful tool for analyzing the complex conformational behavior of biomolecules as obtained from molecular-dynamics trajectories (see Amadei et al., 1993, Balsera et al., 1996, and García, 1992, for concepts, details, and limitations). For the PCA carried out here, all heavy atoms of the peptide backbone were included. In addition, a united-atom representation was introduced for each side chain by assigning a mass equivalent to that of all its constituting atoms, which was located at its center of mass, reducing the number of sites to $N = 38$. Explicit tests indicate that PCA, including all atoms, provides an essentially identical picture for the low-order modes that are of interest, which is in line with previous findings (Aalten et al., 1997). The dependence of the resulting motions upon trajectory length was also carefully evaluated and results were found to be well converged for simulations on the order of 20 ns in duration. For example, the dot product between the slowest motion, i.e., $\{\mathbf{m}_1\}$, computed over two distinct 20 ns trajectories, and that from a 30- to 40 ns trajectory at the lowest temperature, 280 K, is ~0.98—therefore indicating that the modes are essentially converged. Moreover, the dot products between the vectors $\{\mathbf{m}_1\}$ obtained from PCA at all temperatures always exceed 0.98, indicating that this motion, as such, is not temperature-dependent. Finally, the modes discussed in this investigation are found to exist also when using the zwitterionic octapeptide, and in the simulations with a larger solvation sphere around the peptide, as discussed above.

As an alternate approach to using Cartesian coordinates, we have also applied PCA in internal coordinates (see e.g., Aalten et al., 1997). Natural internal coordinates for protein backbone conformational changes are the usual dihedral angles φ and ψ, defining rotations around the C_α-$C_{carbonyl}$ and C_α-N_{amide} bonds of each amino acid, respectively. Concerning the octapeptide, we confirm qualitatively that opening/closing and librational modes in the PCA analysis also exist in φ/ψ space. However, at variance with PCA in Cartesian coordinates (see below for a detailed discussion), there is no single eigenvector that can be used as a reaction coordinate, the reason being that the motions represented by the eigenvectors in dihedral space turn out to be very local in the sense of involving mainly individual

angles and thus decoupled rotations. Therefore, a linear combination of many angular eigenvectors must be used to describe sufficiently collective correlated motion. This is also confirmed by the fact that many more such eigenvectors are needed to represent the variance of the trajectory as compared to performing PCA in Cartesian coordinates, where the first mode already accounts for ~40% of the total variance.

RESULTS AND DISCUSSION

Time evolution and temperature-dependence of structural parameters

To get a first impression of the dynamics of the solvated octapeptide GVG(VPGVG), we consider the time evolution of a few selected quantities describing the overall structure. The first parameter of interest is the distance from the C- to the N-terminus, r_{C-N}, which is a measure of the extension of this short polymer chain. A typical time-evolution profile of this quantity is presented in Fig. 1 *a* at a temperature of 330 K. Judging from this parameter, there are two distinctly different types of peptide structure: the majority of the time r_{C-N} oscillates approximately a distance of 17 Å (corresponding to open structures), whereas a second, less probable configuration is found when $r_{C-N} \approx 5$ Å (stemming from closed structures). Representative configurations, as obtained at 330 K for each type of conformation, are depicted in Fig. 2. The presence of two types of peptide conformations is also mirrored by the radius of gyration of the biopolymer, r_{gyr}, which is a standard measure of a polymer's overall size. This parameter is strongly correlated with the end-to-end distance, r_{C-N} (see Fig. 1 *b*), such that for the extended structures, $r_{gyr} \approx 8$ Å, whereas for the closed ones, $r_{gyr} \approx 4$ Å. As a simple measure of the proximity of hydrophobic side chains of the peptide we also consider the radius of gyration of the valine side chains only, r_{gyr}^{Val} (see Fig. 1 *c*). Again, this parameter is found to be strongly, although not perfectly, correlated with the end-to-end distance and, as expected, the radius of gyration of the entire peptide.

The open and closed structures have distinctly different hydrogen-bond (HB) arrangements as indicated by changes in the numbers of HBs of different classes. Specifically, we consider the number of HBs within the peptide that directly connect amino acid donor (NH) and acceptor (CO) groups, n_{pp}; the number of HBs between the peptide and water molecules in its solvation shell, n_{ps} (*p*eptide-*s*olvence); and the number of water molecules that bridge different parts of the peptide chain by simultaneously forming HBs to two or more nonconsecutive amino acid residues, n_{bw} (see Fig. 2). According to Fig. 1, these quantities are again found to be strongly correlated to r_{C-N}. In the closed state, peptide/peptide HBs and water bridges exhibit values of $\sim n_{pp} \approx 2$–3 and $n_{bw} \approx 2$, respectively, whereas peptide/solvation water interactions amount to $\sim n_{ps} \approx 12$ HBs. This is quite different in the extended state: there are few peptide/peptide HBs, $n_{pp} \approx 0$, and bridging waters, $n_{bw} \approx 0$, but $\sim n_{ps} \approx 16$ peptide/solvation water HBs. These simple parameters—as well as others not depicted here, such as the moments of inertia—indicate several opening and closing events in this trajectory, and thus suggest that the present MD simulations are sufficiently able to sample the conformational space available to the peptide to distinguish between two very different types of structure which are found to be in dynamic equilibrium.

As another measure of the solvation environment of the peptide we consider the number of water molecules within the first solvation shell. This quantity may be broken down into two subclasses: 1), the number of waters solvating the hydrophilic backbone atoms, n_{bb} (*b*ack*b*one); and 2), those that solvate the hydrophobic *s*ide *c*hain carbons, n_{sc} (side chain). The water molecules of the first solvation shell are defined to be within 4.5 Å of the peptide heavy atoms as obtained from the first nearest-neighbor peak of the radial

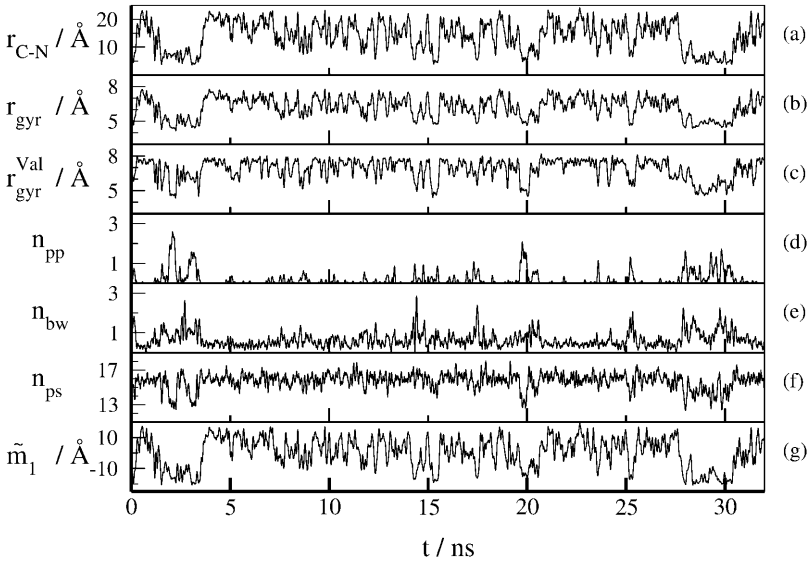

FIGURE 1 Time evolution of selected structural quantities of GVG(VPGVG) in water at 330 K. (*a*) Distance from C- to N-terminus, r_{C-N}; (*b*) radius of gyration, r_{gyr}; (*c*) radius of gyration of the valine side chains, r_{gyr}^{Val}; (*d*) number of peptide-peptide HBs, n_{pp}; (*e*) number of water molecules bridging two amino acids of peptide by HBs, n_{bw}; (*f*) number of HBs between peptide and solvating water molecules, n_{ps}; and (*g*) projection of the trajectory onto the first eigenvector of the covariance matrix, $\tilde{m}_1$; see text for definitions. For presentation purposes only, the functions were denoised using the Savitzky-Golay procedure (Savitzky and Golay, 1964), where a time window of 128 ps and a polynomial of sixth degree was used; the analysis was, however, carried out based on the original data sets.

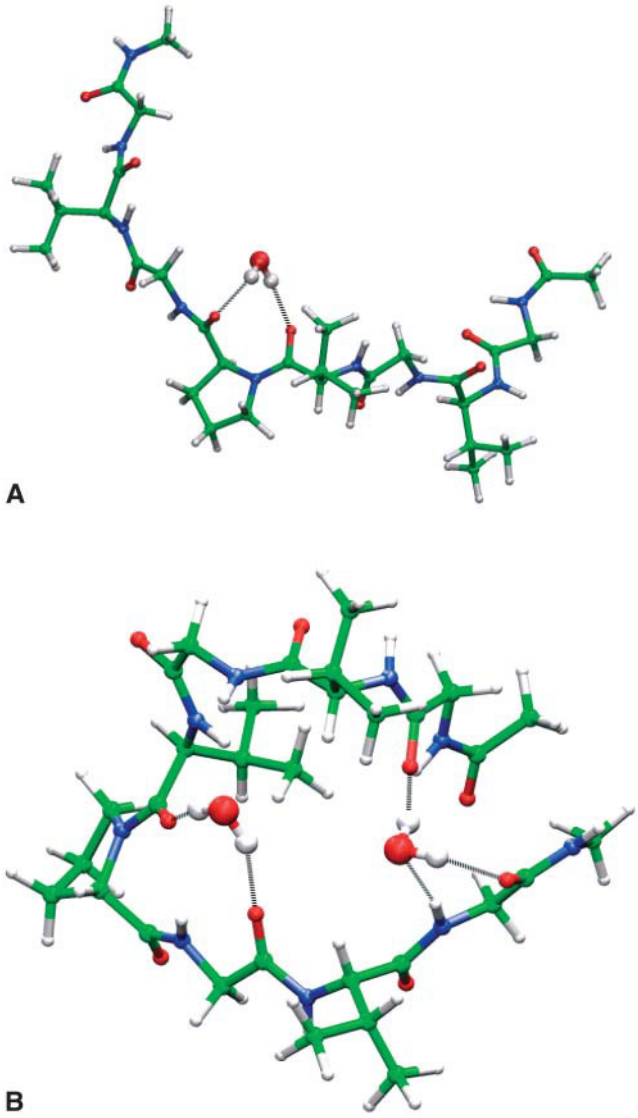

FIGURE 2 Graphical representation of typical protein conformations at 330 K including only bridging waters; (*a*) open state and (*b*) closed state.

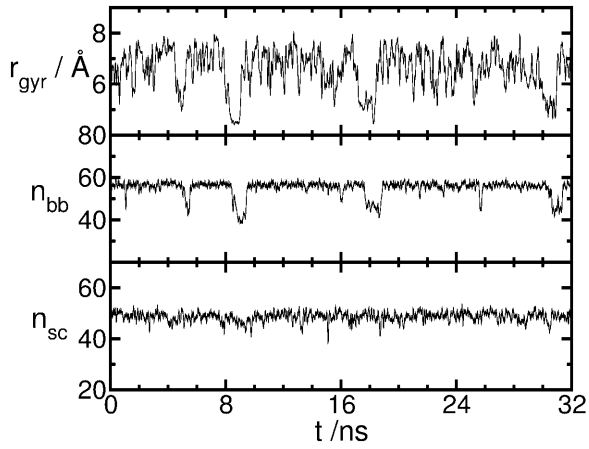

FIGURE 3 Time evolution of selected structural quantities of GVG(VPGVG) in water at 300 K. (*Top*) Radius of gyration, r_{gyr}; (*middle*) number of water molecules in first solvation shell of hydrophilic backbone atoms, n_{bb}; and (*bottom*) number of water molecules in first solvation shell of hydrophobic side chain atoms, n_{sc}. See Fig. 1 for smoothing procedure.

distribution function. For the hydrophobic side chains the first nearest-neighbor peak of the radial distribution function of water oxygen around peptide heavy atoms is within 4.5 Å. For the backbone atoms, the radial distribution function has two maxima in this region, one stemming from the waters associated with the backbone via HB within 3.0 Å, and one belonging to waters which are in the vicinity of the backbone but without an HB at 4.5 Å. Therefore in both cases the reasonable cutoff of 4.5 Å was chosen. For the current small peptide n_{bb} and n_{sc} are roughly equal to ~50–70 water molecules, depending on the temperature. We plot in Fig. 3 the time evolution of these two quantities along with the gyration radius, r_{gyr}, at 300 K. At this temperature we again find that r_{gyr} shows the signature of both open and closed structures, although with pronounced lower occurrence of the latter. As expected, n_{bb} is strongly correlated with the opening and closing, dropping in value by ~20 water molecules upon entering the closed state. This is in stark contrast with the number of waters around the side chains: n_{sc} is largely insensitive to the opening and closing motion. A similar happening is found to occur at all temperatures, which strongly suggests that rearrangement of the water structure around the hydrophobic side chains does not play a dominant role in the energetics of forming open and closed structures.

A similar picture where one observes two types of structures, open and closed, with correlated r_{C-N}, r_{gyr}, and HB types, is also found in simulations where the thickness of the solvating water sphere is increased as well as with alternate peptide chain capping groups at selected temperatures of 280 and 320 K. This gives us confidence that this scenario is not an aberration of our computational methodology. Moreover, in agreement with Reiersen et al. (1998), this latter finding suggests that the results should depend on only the presence of the repeat unit VPGVG itself. We note in passing that the timescale of the peptide backbone fluctuations which interconvert open and closed conformations is on the order of ~1 ns (see Fig. 6 *b*) even for this minimalistic elastin model. The implications of this timescale is that, for MD trajectories on the order of only a few nanoseconds, statistical quantities (which depend on the conformation of the peptide backbone) will be subject to large errors and, hence, should be conservatively interpreted—particularly if longer chains, yielding even longer relaxation times, are investigated.

We now consider how this dynamic equilibrium behaves as a function of temperature. Given the above description of the change in HB configuration as a function of the type of structure, it is convenient to define the number of internal hydrogen bonds, n_{IHB}, as the sum of n_{pp}, and the HB arising

from the bridging waters, n_{bw}. Note that both n_{pp} and n_{bw} exist only when the structure is closed. An average over the entire trajectory will result in very small numbers with large associated errors, whereas n_{IHB} is a more statistically meaningful quantity carrying similar information. The data from the time averages $\langle r_{C-N}\rangle$, $\langle r_{gyr}\rangle$, $\langle n_{IHB}\rangle$, $\langle n_{ps}\rangle$, and $\langle r_{gyr}^{Val}\rangle$ are plotted in Fig. 4 as a function of temperature. As expected from the above correlations $\langle r_{C-N}\rangle$, $\langle r_{gyr}\rangle$, $\langle n_{IHB}\rangle$, and $\langle r_{gyr}^{Val}\rangle$ display a similar temperature-dependence which may be classified in terms of two distinct temperature regimes below and above a temperature close to 330 K. The average end-to-end distance increases slightly from 280 K to 310 K, where a significant decrease of $\langle r_{C-N}\rangle$ sets in with a maximum contraction at 330 K, followed by a rise in value up to 390 K. Similarly, $\langle n_{IHB}\rangle$ and $\langle r_{gyr}\rangle$ mirror this trend. The average of the radius of gyration stemming from the valine side chains only, $\langle r_{gyr}^{Val}\rangle$, also shows an initial decrease, but at variance with the total radius of gyration it remains small up to high temperatures subject to sizable fluctuations. Below 330 K the structures have slightly larger $\langle r_{gyr}\rangle$ and only a few internal HBs, which is consistent with only a small percentage of closed structures. The largest number of closed structures is observed at 330 K, resulting in the smallest $\langle r_{gyr}\rangle$ and the largest $\langle n_{IHB}\rangle$. Above this temperature, $\langle r_{gyr}\rangle$ slowly increases in parallel to a decrease in $\langle n_{IHB}\rangle$, which is consistent with a decrease in the number of closed structures. Both $\langle n_{pp}\rangle$ and $\langle n_{bw}\rangle$ also follow this same trend, although with much larger numerical noise. Overall, our picture not only is consistent with the interpretation of an ITT occurring at ~330 K but we also find a slow trend reversal at higher temperatures.

As a measure of how the peptide/water interface behaves during these structural transitions, the total number of interfacial HBs, $\langle n_{ps}\rangle$, and the numbers of waters solvating the backbone and side-chain atoms, $\langle n_{bb}\rangle$ and $\langle n_{sc}\rangle$, respectively, are considered (see Fig. 4 *d*). There is a continuous decrease in $\langle n_{ps}\rangle$ and $\langle n_{bb}\rangle$ observed upon increasing the temperature with a pronounced kink at ~330 K. The trend obtained from averaging the structural quantity, n_{ps}, is much less pronounced and is examined in greater detail in the section on HB dynamics and kinetics by dynamical analysis of the peptide/water interfacial HBs. This hints that the peptide/water interface also exhibits two temperature regimes, as already observed for the structural quantities associated with the peptide structure. This is not true, however, for $\langle n_{sc}\rangle$, which decreases approximately linearly across the entire temperature range; i.e., consistent with a decrease caused by increased thermal fluctuations at

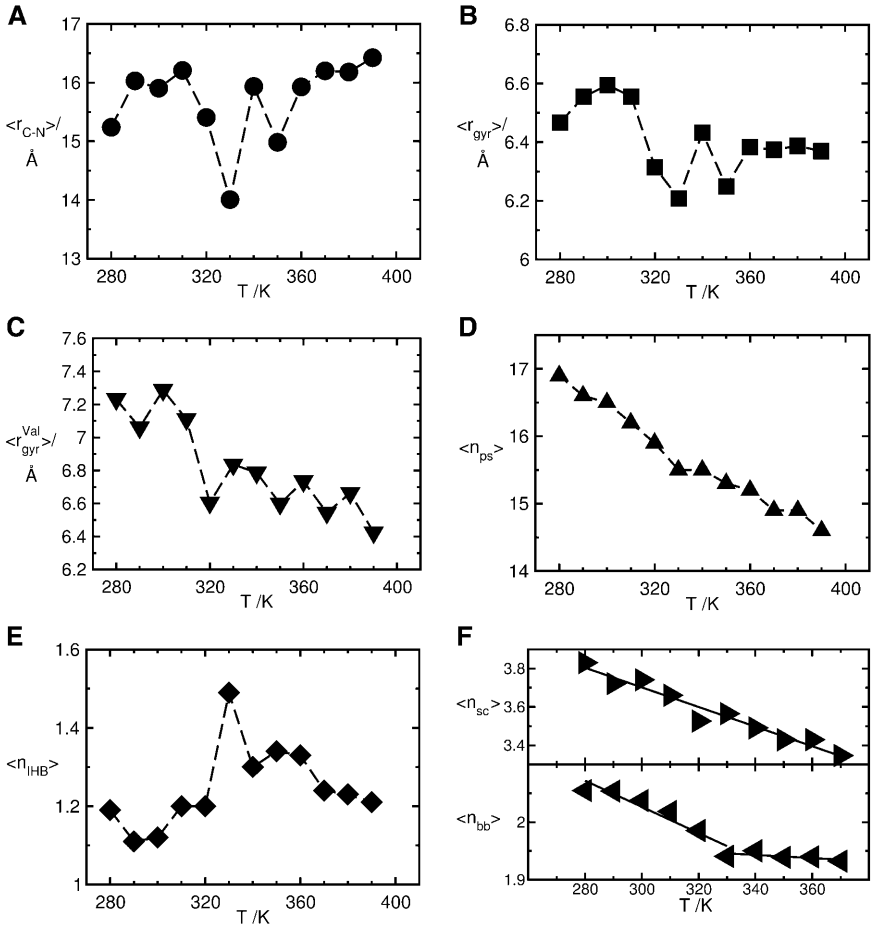

FIGURE 4 Average quantities as a function of temperature. (*a*) Distance from C- to N-terminus, r_{C-N}, ●; (*b*) radius of gyration, r_{gyr}, ■; (*c*) radius of gyration of valine side chains, r_{gyr}^{Val}, ▼; (*d*) number of HBs between peptide and solvating water molecules, n_{ps}, ▲; (*e*) number of internal HBs, n_{IHB}, ♦; and (*f*) number of water molecules solvating a backbone heavy atom, n_{bb}, ▶; and number of water molecules solvating a hydrophobic side-chain atom, n_{sc}, ◀; see text for definitions. Dashed lines are linear connections of the data to guide the eye. Solid lines are linear least-squares fit.

higher temperature. Thus, although the structure of the peptide/water interface is changing concurrently with the peptide transitions, it is only true for the solvent structure around the backbone atoms.

Overall, these averaged structural quantities provide a suggestive, though by no means comprehensive, picture of the atomic-level details of the peptide structural transitions. The presence of two types of structures, open and closed, correlates extremely well with the observation of an isodichroitic point in the CD spectra (Nicolini et al., 2004; Reiersen et al., 1998) and supports the description of this small peptide as behaving like a two-state system. The increase of the contribution of closed structures, at temperatures up to 330 K and its subsequent decrease at higher temperatures, is consistent with the temperature-dependence of more compact structures containing γ- and β-turns, as observed in the FT-IR spectra of the complementary experimental investigation (Nicolini et al., 2004). The differential scanning calorimetry (DSC) and pressure perturbation calorimetry (PPC) thermodynamic measurements presented in the joint experimental study may also be interpreted as the peptide ultimately reverting to a structurally and thermodynamically similar state at temperatures near the normal boiling point of water. In addition, the above scenario is qualitatively in accord with that presented in Li et al. (2001b), which describes the ITT using a similar but much longer model peptide. Specifically this study also finds an increasing number of peptide/peptide HBs, an overall average contraction of the peptide at the ITT, a decreasing number of interfacial water molecules, and an increasing number of bridging waters which may be thought of as the internal waters in our small elastin-like analog. The authors of Li et al. (2001b) attribute this shrinkage to a hydrophobic collapse, which is in agreement with our observed temperature-dependence of $\langle n_{\mathrm{ps}} \rangle$ and $\langle r_{\mathrm{gyr}}^{\mathrm{Val}} \rangle$.

However, the current picture suggests the subtle, but crucial, difference that the observed structural transitions in capped GVG(VPGVG) are not caused by a classical textbook hydrophobic collapse. Rather, there is a net exchange of peptide/peptide and bridging-water intramolecular HBs for peptide/water interfacial HBs; the energetic implications of the various HB types are addressed in the section on HB dynamics and kinetics. For the octapeptide, our finding and its interpretation has a striking resemblance to the findings concerning self-association of methanol in water in Dixit et al. (2002), in addition to being in qualitative accord with some concepts of hydrophobic solvation as reviewed in Pratt and Pohorille (2002). We must stress, however, that the peptide model in this previous study has a solvation structure where ~80% of the solvating water molecules are located around hydrophobic side chains in contrast to the ~50% observed in our much smaller system. Thus, it remains an open issue to address these questions in the case of longer GVG $(\mathrm{VPGVG})_{\mathrm{n}}$ peptides. In the following two subsections these suggestive findings, which are based on simple descriptors, will be further scrutinized by a detailed statistical-mechanical analysis.

Principal component analysis and order parameter

To probe the above findings in a systematic but simple way one would ideally wish to describe these phenomena by a single parameter, i.e., by an order parameter or reaction coordinate. We have employed the PCA to explore this possibility (Amadei et al., 1993; Balsera et al., 1996; García, 1992; Hyvärinen et al., 2001) for presentations of this technique. In this approach one computes, by time averaging, $\langle \ldots \rangle$, over the entire MD trajectory the covariance matrix $\mathbf{C} = \left\langle [\mathbf{x}(t) - \langle \mathbf{x} \rangle][\mathbf{x}(t) - \langle \mathbf{x} \rangle]^{\mathrm{T}} \right\rangle$, where $\mathbf{x}(t)$ are the Cartesian coordinates of the peptide atoms at time t in a frame of reference where the overall translations and rotations of the polymer have been subtracted. The $3N$–6 normalized eigenvectors, $\{\mathbf{m}_{\mathrm{i}}\}$, with nonzero eigenvalues, $\{\lambda_{\mathrm{i}}\}$, provide a basis in which the complex polypeptide motion may be decomposed. This then provides a theoretical framework which can be thought of as being analogous to harmonic normal modes that are of ubiquitous use to explain spectroscopic observations of small molecules. In practice, this allows us to disentangle relevant peptide backbone folding motions from small-amplitude vibrations via projecting the deviations of the MD trajectories from the average structure onto the eigenvectors, i.e., $\tilde{m}_{\mathrm{i}} = [\mathbf{x}(t) - \langle \mathbf{x} \rangle]\mathbf{m}_{\mathrm{i}}$. Ideally, for uncorrelated small-amplitude vibrations the corresponding projections $\tilde{m}_{\mathrm{i}}$ will simply fluctuate around an average value yielding an approximately Gaussian distribution function, $P(\tilde{m}_{\mathrm{i}})$; the width might be temperature-dependent akin to harmonic molecular vibrations. Strong deviations from such a unimodal behavior would single out interesting modes that can be associated to collective changes involving many atoms. Upon changing the temperature the various modes are expected to mix, particularly the higher-order modes. Thus, a common basis, $\{\mathbf{m}_{\mathrm{i}}\}$, has to be chosen to ensure a consistent analysis. In the following, projections $\tilde{m}_{\mathrm{i}}$ will be performed onto the basis of eigenmodes of the low-temperature trajectory at 280 K. In addition, the mass weighted covariance matrix $\mathbf{C}' = \mathbf{M}^{1/2}\mathbf{C}\mathbf{M}^{1/2}$ provides a crude and very approximate method (Andriciolaei and Karplus, 2001; Schlitter, 1993) for estimating the (vibrational/librational) entropy contribution of each mode by assuming a superposition of independent one-dimensional quantum harmonic oscillators, as

$$S_{\mathrm{ho}} = k_{\mathrm{B}} \sum_{\mathrm{i}}^{3\mathrm{N}-6} \left\{ \frac{\hbar\omega_{\mathrm{i}}/k_{\mathrm{B}}T}{e^{\hbar\omega_{\mathrm{i}}/k_{\mathrm{B}}\mathrm{T}} - 1} - \ln(1 - e^{-\hbar\omega_{\mathrm{i}}/k_{\mathrm{B}}\mathrm{T}}) \right\}, \quad (1)$$

where the (quasiharmonic) frequencies $\omega_{\mathrm{i}} = \sqrt{(k_{\mathrm{B}}T/\lambda'_{\mathrm{i}})}$ are obtained from the eigenvalues λ'_{i} of $\mathbf{C}'$; k_{B} is the Boltzmann constant.

Upon projecting the MD trajectories onto the eigenvector

with the largest eigenvalue, λ_1, it is found that this mode, $\mathbf{m}_1$, actually describes the opening and closing motion of the octapeptide, and is present at all temperatures (see Fig. 5 *a* for a graphical illustration). In Fig. 1 *g*, we depict this projection, $\tilde{m}_1$, as a function of time at 330 K where it can be inferred to be perfectly correlated with the other parameters already discussed in the previous section. The octapeptide thus exists in a closed state, $\tilde{m}_1 \approx -22\,\mathring{A}$, with end-to-end distances of ~5 Å; and an extended state, $\tilde{m}_1 \approx +5\,\mathring{A}$, with end-to-end distances of ~17 Å. In addition, the projection process yields for $\tilde{m}_1$ a bimodal distribution function $P(\tilde{m}_1)$ at low temperatures, whereas it adopts a unimodal, but very broad and skewed shape upon heating (see Fig. 5 *c*).

The mode with the next largest eigenvalue, $\mathbf{m}_2$, can be classified as a peptide backbone librational mode (see Fig. 5 *b* for a sketch). During this motion the peptide backbone undergoes twisting, which is actually very similar in spirit to that described for the deformation of β-turns in Li et al. (2001b) and Urry (1997). In contrast to the lowest-order projections, however, $\tilde{m}_1$ and $\tilde{m}_2$(as well as all other higher-order mode projections of the peptide backbone) are characterized by fairly symmetric, narrow, and unimodal distributions $P(\tilde{m}_i)$ that are essentially temperature-independent (see Fig. 5 *d*). This implies that—as far as the interpretation of the behavior of the folding transitions are concerned—we are able to neglect all backbone librational motions and reduce our considerations down to only a single degree of freedom: $\mathbf{m}_1$. Thus, we may confidently employ the corresponding projection $\tilde{m}_1$ as a natural many-body collective reaction coordinate, or order parameter, for investigating the folding transition dynamics of GVG (VPGVG) in water.

Having obtained a proper order parameter distribution function, $P(\tilde{m}_1)$, allows one to readily define an effective relative free energy profile (or potential of mean force) according to $\Delta F(\tilde{m}_1) = -k_B T \ln[P(\tilde{m}_1)/P(\tilde{m}_1^{\mathrm{ref}})]$ as a function of temperature. The normalizing reference value $P(\tilde{m}_1^{\mathrm{ref}})$ is chosen such that the arbitrary value at the minimum of the free energy profile is set to zero for convenience (see Fig. 5 *e*). At 280 K, the free energy shows two minima, separated by a small barrier, related to both open (broad global minimum at $\tilde{m}_1 \approx 5\,\mathring{A}$) and closed (local minimum at $\tilde{m}_1 \approx -20\,\mathring{A}$) structures with the latter ~3 kJ/mol higher in energy then the former. By 330 K the minimum associated with the closed structure, as well as the barrier, become much lower in relative free energy; thus the entire profile of ΔF broadens out into a flat potential energy landscape. Above 330 K the free energy of the closed minimum gradually increases again and eventually disappears by 370–390 K. Performing an identical analysis for the remaining modes

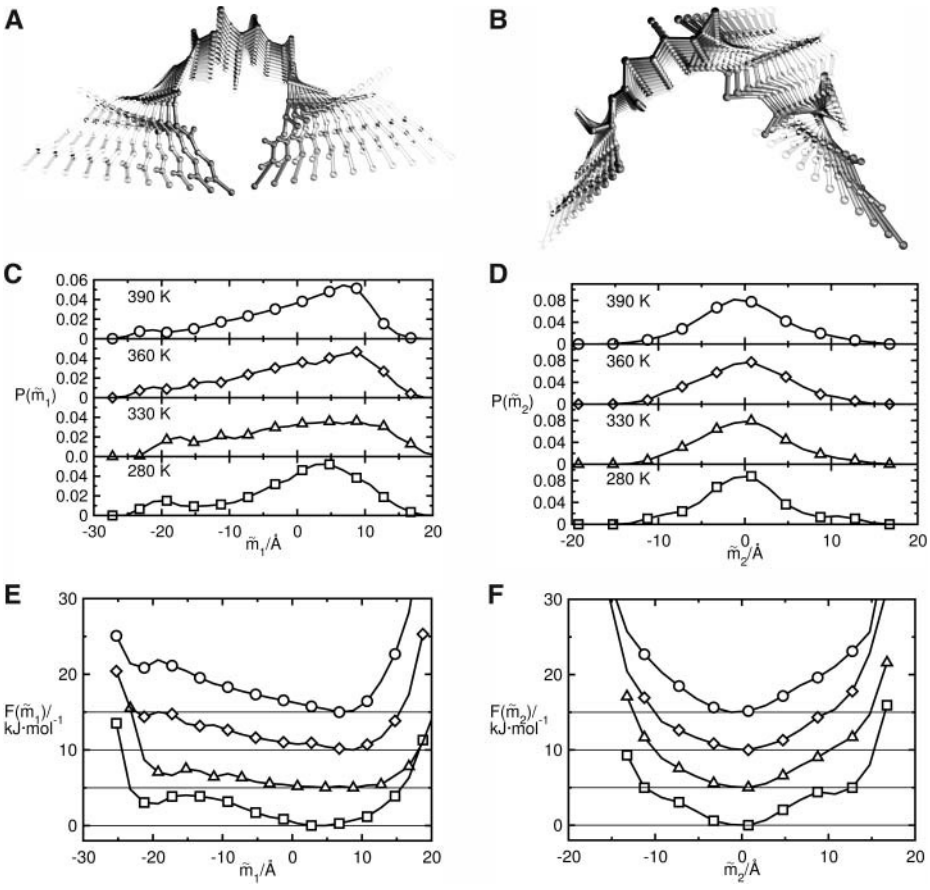

FIGURE 5 Results of the principal component analysis. (*a*) Visualization of large amplitude opening and closing mode, $\mathbf{m}_1$. (*b*) Visualization of large amplitude librational mode, $\mathbf{m}_2$. (*c*) Distribution function of the projection $\tilde{m}_1$ at 280, 330, 360, and 390 K. (*d*) Distribution function of the projection $\tilde{m}_2$ at 280, 330, 360, and 390 K. (*e*) Relative free energy along the projection $\tilde{m}_1$. (*f*) Relative free energy along the projection $\tilde{m}_2$. In *a* and *b*, an artificial trajectory using the full first $\mathbf{m}_1$ (*a*), and second $\mathbf{m}_2$ (*b*), eigenvector was synthesized for a suitable graphical presentation. In *e–f*: 280 K, □; 330 K, △; 380 K, ◇; and 390 K, ○. For presentation purposes the free energy profiles for 330, 380, and 390 K were shifted in energy by 5, 10, and 15 kJ mol^{-1}, respectively.

provides approximately harmonic potentials of mean force (see Fig. 5 *f* for the potential derived from $\tilde{m}_2$, in agreement with our use of only $\tilde{m}_1$ as an order parameter). The trend in $\Delta F(\tilde{m}_1)$ reflects the presence of the temperature regimes observed from the average parameters, i.e., increased folding from 280 to 320 K, the observation of maximum folded structures ~330 K, and the unfolding at $T \geq 340$ K. The presence of two minima in $\Delta F(\tilde{m}_1)$ in conjunction with the temperature-induced changes naturally explains the existence of the isosbestic and isodichroitic points observed in FT-IR and CD experiments (Nicolini et al., 2004), respectively, and gives us confidence in the reliability of our simulations.

At 330 K, fluctuations and thus statistical errors are larger than at other temperatures due to the broader configuration space which must be sampled possibly in conjunction with slower relaxation. This effect is similar to the slowing-down problem occurring for statistical convergence at second-order phase transitions where all quantities, and in particular the order parameter itself, undergo large fluctuations. However, the finite system size does not allow for a true phase transition with a well-defined transition temperature but rather, one observes, in agreement with spectroscopic and thermodynamic measurements (Nicolini et al., 2004; Reiersen et al., 1998; E. Schreiner, C. Nicolini, B. Ludolph, R. Ravindra, N. Otte, A. Kohlmeyer, R. Rousseau, R. Winter, and D. Marx, unpublished material) the two temperature regimes which are bracketed around the temperature of maximal folding, $T \approx 330$ K.

The dynamical motion of the peptide itself can be analyzed by examining the time-dependence of the reaction coordinate $\tilde{m}_1$ as described by the correlation function $c_m(t) = \langle \tilde{m}_1(0)\tilde{m}_1(t)\rangle / \langle \tilde{m}_1(0)\tilde{m}_1(0)\rangle$ (see Fig. 6 *a*). This time-autocorrelation function may be well approximated in the short time limit, $t < 100$ ps, by an exponential function, $c_m(t) \sim \exp[-t/\tau_m]$, with an associated relaxation time, τ_m, of the peptide's opening and closing motion. The temperature-dependence of this important dynamical parameter is depicted in Fig. 6 *b*. For temperatures <330 K, $\tau_m \approx 300$–350 ps is roughly constant within the accuracy of our statistics. Above 330 K, there is a progressive speedup ($\tau_m \approx$ 130–150 ps) which reflects the steepening of the free energy surface in the region of closed structures, i.e., for $\tilde{m}_1 \ll 0$. From 370–390 K, where the free energy surface contains essentially a single minimum, $\tilde{m}_1 \approx +5$, with approximately constant curvature, the relaxation time levels off to a plateau value of $\sim\tau_m \approx 150$ ps. Temperature variations of τ_m thus reflect three dynamical scenarios corresponding to *folding*, *unfolding*, and *unfolded*, which is slightly different from the observations made on the average structural quantities. Note, however, that the last of the three temperature regimes represents a limiting case of the unfolding transition, where a minimum for closed structures no longer effectively exists.

These findings correlate well with larger peptide backbone fluctuations observed in NMR spectroscopy (Perry et al., 2002) for water-swollen elastins. Unfortunately, the most directly comparable NMR measurements of ^{13}C relaxation times for poly(GVGVP) in solution are only obtained for the temperatures below the ITT (Kurková et al., 2003). Nonetheless, the authors report a mean effective correlation time for polymer motion on the order of ~500 ps at 298 K in astonishing agreement with the 300-ps timescale reported here at the same temperature. These facts suggest that temperature-dependent measurements of NMR ^{13}C relaxation times for this small system may serve as an independent verification of our findings.

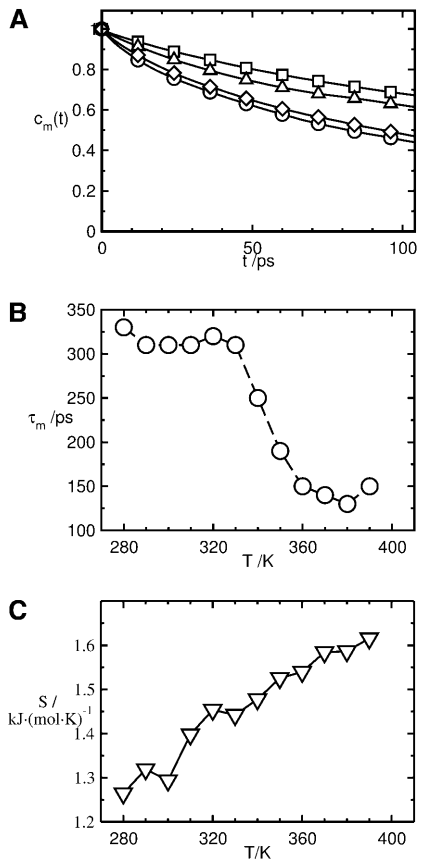

FIGURE 6 Dynamics of the $\mathbf{m}_1$ eigenmode. (*a*) Autocorrelation function, $c_m(t)$, at 280 K, □; 330 K, △; 360 K, ◇; and 390 K, ○. (*b*) Relaxation time τ_m as a function of temperature; here the symbol size reflects approximate error bars, ○. (*c*) Peptide backbone quasiharmonic entropy, *S*, ▽, as a function of temperature; see text for definitions.

Previous MD studies on much larger poly(VPGVG) chains find qualitatively that the peptide becomes ''slightly more dynamic,'' or less rigid at higher temperatures (Li et al., 2001b). This also matches our quantified speedup of the dynamics of the peptide's backbone opening and closing motion. Thus, despite the increase in number of peptide/peptide HBs, there must be an overall increase of freedom in the motion of the peptide backbone. The question then arises: does this extra motion lead to favorable entropic contribution to the ITT from the peptide? To address this, we consider the entropy change of the peptide backbone motion as estimated

from a quasiharmonic approximation based on the principal component analysis (Andriciolaei and Karplus, 2001; Schlitter, 1993). Note that this analysis is based on a quasiharmonic approximation (Andriciolaei and Karplus, 2001; Schlitter, 1993), whereas the lowest-order mode, $\mathbf{m}_1$, which contributes ~40% to the overall variance of the peptide backbone, is strongly anharmonic and even bimodal at low temperatures. However, its contribution to the total peptide backbone entropy is fairly small, with much larger contributions arising from the more harmonic higher-order modes. Fig. 6 *c* shows the entropy of the peptide in a united-atom representation as a function of temperature. We find that despite the volume contraction of the peptide <330 K the entropy is increasing with rising temperature, i.e., the entropy of the peptide itself increases upon folding. The associated entropy change is also consistent in magnitude with the experimentally measured entropy increase of 0.15 kJ/mol^{-1} K^{-1} and 0.11 kJ/mol^{-1} K^{-1} (at 298 K and 1 bar) obtained from a van't Hoff analysis of equilibrium constants of both CD and FT-IR data (Nicolini et al., 2004; Reiersen et al., 1998; E. Schreiner, C. Nicolini, B. Ludolph, R. Ravindra, N. Otte, A. Kohlmeyer, R. Rousseau, R. Winter, and D. Marx, unpublished material). These findings are similar in spirit to various librational entropy models employed to explain viscoelastic properties of elastin and its synthetic mimetica (Debelle and Tamburro, 1999; Urry, 1993; Urry et al., 2002). Our analysis does not eliminate the possibility that stabilizing entropic terms from the water are also important contributors to the folding behavior; however, our simulations clearly demonstrate that our elastin mimic is a very dynamical entity and that the thermodynamic consequences of this motion, in particular the increasing entropy, are key components in understanding its structural transitions.

Hydrogen-bond dynamics and kinetics

To address the role of water, and in particular, the influence of hydrogen bonding on the peptide's conformational transitions, we analyze the dynamics of the HB network. To this end, we employ the intermittent HB autocorrelation function (Chandra, 2000; Luzar and Chandler, 1996a,b; Starr et al., 1999; Stillinger, 1975; Xu and Berne, 2001), $c(t) = \langle h(0)h(t)\rangle/\langle h\rangle$. As usual the HB population variable $h(t)$ is defined to be unity, $h(t) = 1$, if a particular HB exists at time t and zero $h(t) = 0$ otherwise (the criteria to define an HB are compiled and discussed in Methods, Models, and Technical Details); and the average $\langle \ldots \rangle$ is taken over all HBs that were present at time $t = 0$. This function describes the probability that an HB, which was intact at $t = 0$, is intact at time t independent of possible breakings (and reformation) in the interim time. Similar to the average number of HBs introduced above, the following classes were defined: HBs between water molecules in the bulk $c_w(t)$ (Fig. 7 *a*); between water molecules which are both located within the first solvation shell of the hydrophobic side chains $c_{sc}(t)$; between first shell protein solvation water and bulk water $c_{sw}(t)$ (Fig. 7 *b*); between the peptide and first shell solvation water $c_{ps}(t)$ (Fig. 7 *c*); and direct HB contacts of the peptide with itself $c_{pp}(t)$ (Fig. 7 *d*). These functions provide us with a wealth of insights into the complex dynamics and the associated timescales of the solvated peptide in relation to, e.g., relaxation dynamics in bulk water. Comparison of $c_w(t)$ and $c_{ps}(t)$ nicely shows the well-known trend (Tarek and Tobias, 1999, 2002a,b) of slower dynamics for interfacial peptide water HBs than those within bulk water: depending on the temperature, $c_w(t)$ and $c_{ps}(t)$ decay to zero between 10–20 ps and 20–50

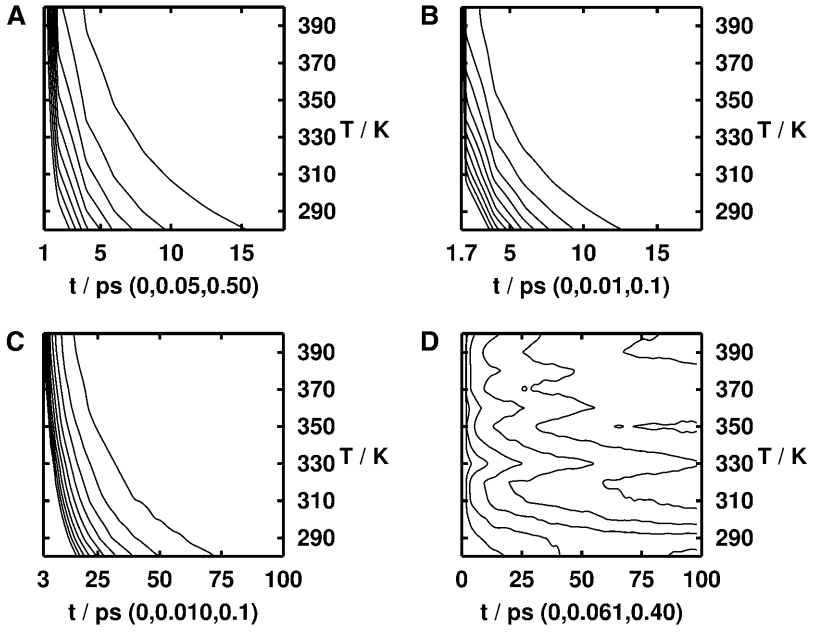

FIGURE 7 Temperature- and time-dependence of various HB autocorrelation functions, $c(t)$: HBs between (*a*) water molecules in the bulk, $c_w(t)$; (*b*) first shell solvation water molecules and bulk water molecules, $c_{sw}(t)$; (*c*) the peptide and first shell solvation water molecule, $c_{ps}(t)$; and (*d*) direct HB contacts of the peptide with itself, $c_{pp}(t)$ (see text for definitions). The choice of contour lines is coded in each panel as *a*, *b*, and *c*, where *a* and *c* denote the lowest and the highest contours, respectively, and *b* defines the relative spacing.

ps, respectively, at temperatures <330 K. At the highest temperatures both functions decay to zero within 10 ps with the most pronounced speedup of this process occurring at the peptide/water interface. The functions $c_w(t)$ and $c_{sc}(t)$ are virtually identical, and hence the latter is not shown. Conversely, the function $c_{sw}(t)$ decays to zero in only a few picoseconds at all temperatures, indicating that only fast HB breaking dynamics occurs for this class of bonds. A curiosity is the function $c_{pp}(t)$, which instead of decaying to zero still retains a finite value for upwards of 100 ps or more. This behavior arises from the fact that peptide/peptide HBs, once broken, cannot diffuse away from each other inasmuch as they are formed involving the peptide backbone; i.e., they have a finite probability to reform even after long elapsed times due to topology.

To extract further information on the processes occurring on these various timescales we make use of a more elaborate correlation function (Chandra, 2000; Luzar, 2000; Luzar and Chandler, 1996a,b; Starr et al., 1999; Xu and Berne, 2001), $n(t) = \langle h(0)[1-h(t)]H(t)\rangle/\langle h\rangle$. This function $n(t)$ measures the conditional probability that an HB, which was intact at $t = 0$, is broken at time $t > 0$, given that the donor/acceptor pair that established the HB at $t = 0$ is still close enough at time $t > 0$ to again potentially form the HB. The function $H(t)$ is at unity only if the HB pair distance is smaller than a cutoff distance of 3.6 Å, which is the second nearest-neighbor shell of the donor/acceptor pair radial distribution function. Thus, $n(t)$ allows one to focus on the dynamics for $t \gtrsim 2$ ps where the HB dynamics is more complex due to its coupling to translational diffusive motion (Luzar, 2000; Luzar and Chandler, 1996a,b), whereas the time domain for $t \lesssim 2$ ps is dominated by fast librational and possibly vibrational motion of water molecules. This function plays a significant role for two types of HBs considered in this work: 1), HBs between water molecules in the bulk, $n_w(t)$ (Fig. 8 *a*), and 2), HBs between the peptide and water molecules in its first solvation shell, $n_{ps}(t)$ (Fig. 8 *b*). In both cases, $n(t)$ increases from $t = 0$ in view of the formation of non-hydrogen-bonded pairs resulting from initial HB breaking, up to a maximum point, and then it decreases steadily to zero as the probability of reforming the HB decreases due to diffusion. Comparison of Fig. 8, *a* and *b*, shows a more rapid decay for $n_w(t)$ than $n_{ps}(t)$, which is due to the slower dynamics of HBs at the peptide/water interface.

Following previous studies (Luzar, 2000; Luzar and Chandler, 1996a,b), we formulate a rate equation describing the kinetics of HBs as a combination of terms resulting from breaking and reforming HBs,

$$-\frac{dc(t)}{dt} = kc(t) - \tilde{k}n(t), \tag{2}$$

where k is the rate constant of HB breaking and $\tilde{k}$ is that for HB reformation subsequent to breaking; note that $\tau = 1/k$ defines an average HB lifetime. For bulk water (see Fig. 9 *a* and Table 1), both time constants k_w and $\tilde{k}_w$ show a simple Arrhenius or classical transition-state-theory behavior, i.e., $k = A\exp[-E^{\ddagger}/k_BT]$, at all temperatures (with $E_w^{\ddagger} \approx 7\,\mathrm{kJ/mol}$ and $\tilde{E}_w^{\ddagger} \approx 5$ kJ/mol). Thus, both HB breaking and reformation increase in rate constantly with temperature in the bulk, as expected for a simple thermal process. Note that the bulk water value of k_w at 300 K is close to data from simulations of pure water at room temperature (Luzar, 2000; Luzar and Chandler, 1996a,b; Xu and Berne, 2001), whereas our value of $\tilde{k}_w$ is smaller by a factor of approximately one-half. Although some of this discrepancy may arise from systematic errors as already discussed, it is more likely due to the difference in the dynamical properties of TIP3P water from SPC or SPC/E models (see van der Spoel et al., 1998, and references therein) used in previous studies (Luzar, 2000; Luzar and Chandler, 1996a,b; Xu and Berne, 2001). In particular, TIP3P water has a larger diffusion coefficient (van der Spoel et al., 1998) that allows the water molecules to diffuse away at a different rate after an HB breaking event. Although the bulk water behaves in an expected manner the same cannot be said for HBs that connect the peptide to its surrounding water shell. As with the average structural parameters and the peptide backbone relaxation time, both k_{ps} and $\tilde{k}_{ps}$ show two distinct Arrhenius temperature regimes bracketed ~330 K. Below 320 K the activation energy $E_{ps}^{\ddagger} \approx 12\,\mathrm{kJ/mol}$ to break an interfacial HB is higher than that in the bulk, whereas above 330 K it is much lower (≈4 kJ/mol). Concurrently, HB reforming at the interface

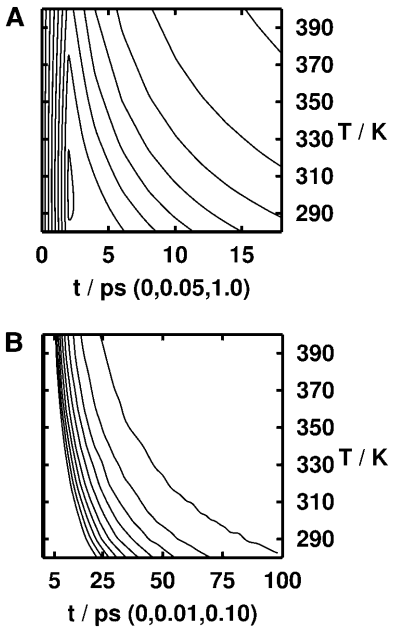

FIGURE 8 Temperature- and time-dependence of various HB autocorrelation functions, $n(t)$: HBs between (*a*) water molecules in the bulk, $n_w(t)$, and (*b*) the peptide and first shell solvation water molecules, $n_{ps}(t)$. See text for definitions. The choice of contour lines is coded in each panel as *a*, *b*, and *c*, where *a* and *c* denote the lowest and the highest contours, respectively, and *b* defines the relative spacing.

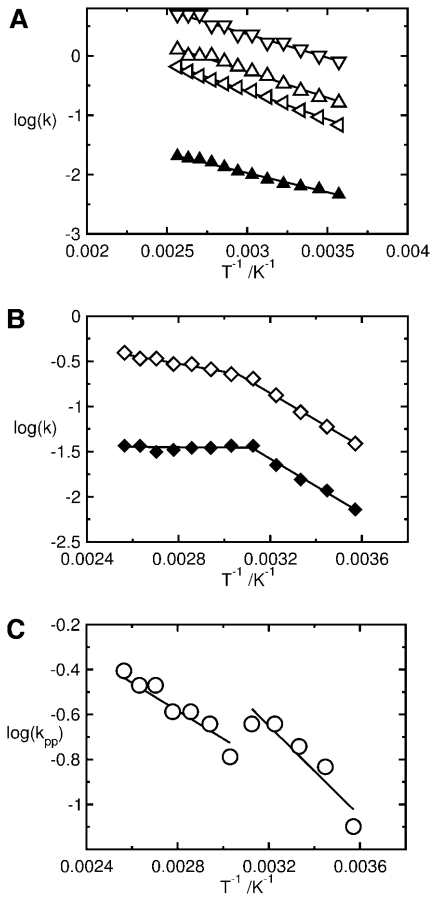

FIGURE 9 Arrhenius plot of rate constants for HB breaking, k, and reformation, $\tilde{k}$, for HBs between (*a*) first shell protein solvation water molecules and bulk water molecules, k_{sw},▽; first shell protein solvation water molecules around the hydrophilic side chains, k_{sc}, △; water molecules in the bulk, k_w, ◁, and $\tilde{k}_w$, ▲; (*b*) the peptide and first shell solvation water molecules, k_{ps}, ◇; and $\tilde{k}_{ps}$, ◆; (*c*) the peptide with itself, k_{pp}, ○. The symbol size covers the error bars and the lines are linear (i.e., Arrhenius) fits; see text for definitions and Table 1 for the resulting fit parameters.

($\tilde{E}^{\ddagger}_{ps} \approx 11$ kJ/mol) is close to that for breaking, but at 330 K the apparent activation energy ($\tilde{E}^{\ddagger}_{ps} \approx 0$ kJ/mol) vanishes. In terms of rates (see Fig. 9), both processes to break and reform HBs at the peptide/water interface effectively slow down upon heating (with regard to a linear Arrhenius-extrapolation of the low temperature behavior) once a critical threshold, ~320–330 K, is surmounted. Hence, the rate to make interfacial HBs essentially reaches a plateau value above 330 K, whereas the one to break these bonds continues to grow with temperature (see Fig. 9).

As mentioned above, the function $c_{sc}(t)$ is almost identical to that of bulk water. As a result, the values of k_{sc} obtained from this function are only slightly larger then those for breaking HBs in bulk water. The temperature-dependence of k_{sc} shows a perfect Arrhenius behavior over the entire temperature range with an activation barrier, $E^{\ddagger}_{sc} \approx 10\,\mathrm{kJ/mol}$, identical to that for the bulk. Thus, in accord with the analysis of average quantities above, the temperature-dependence of the free energy and dynamics of the waters solvating the hydrophobic side chains may be accounted for by strictly thermal fluctuations. Hence, there is no indication that a hydrophobic collapse, resulting from changes in the free energy of the solvation shell of waters around the side chains, is operative in this small peptide.

Conversely, the observation of a profound change in the dynamics of the peptide/water interface is in qualitative accord with thermodynamic measurements (Nicolini et al., 2004; E. Schreiner, C. Nicolini, B. Ludolph, R. Ravindra, N. Otte, A. Kohlmeyer, R. Rousseau, R. Winter, and D. Marx, unpublished material; Urry et al., 2002). In particular, the behavior of the thermal expansion coefficient also indicates an overall decrease in the strength of these interactions. This is also consistent with the proposed hydrophobic collapse that occurs for the ITT of elastins (Li et al., 2001b). However, the most intriguing aspect of the present observation is that the peptide/water HB dynamics, which occur on a timescale of 1–10 ps, mirrors the dynamics of the peptide which occur on timescales two orders-of-magnitude larger.

We now investigate the dynamics of the HBs between interfacial water and bulk water as well as those involving the bridging waters. For the latter class a correlation function $c_{bw}(t)$ is introduced based on an HB population function $h_{bw}(t)$ which is unity only if a water molecule is simultaneously bound to two or more different residues of the peptide. For the former of these two HB classes the second term in Eq. 2 may be neglected due to the relatively rapid decay of $c_{sw}(t)$ to zero. We find that k_{sw} features essentially an Arrhenius behavior at all temperatures, with a similar value of $E^{\ddagger}_{sw} = 7\,\mathrm{kJ/mol}$ as bulk water (see Fig. 9 *a* and Table 1). This picture is entirely in accord with the proposition that these surface water molecules have a hindered orientation which strains the HBs that are formed with bulk water. This does not allow for HB reformation after breaking, hence the process of fast HB reformation does not occur for this class of HBs. In passing, we note that it was discovered recently by femtosecond spectroscopy that the addition of simple salts (such as $Mg(ClO)_4$, $Na(ClO)_4$, and Na_2SO_4) had no influence on the rotational dynamics of water molecules outside the first solvation shells of the ions (Omta et al., 2003). Concerning the octapeptide, it is more surprising that the correlation function of the bridging waters, $c_{bw}(t)$, essentially decays to zero within 2 ps at all temperatures (not shown for that reason). For this small peptide it may thus be concluded from the dynamics that, although water-mediated peptide/peptide bridges (''internal water'') do occur, they play no key stabilizing role for the folded state. As a corollary, for the above assertion of interchange of HBs to be at the heart of the folding/unfolding behavior of elastin, the stability of the folded state must then come from the peptide/peptide HBs.

We thus turn our focus to the function c_{pp}, which describes the dynamics of the peptide/peptide HBs. Unfortunately, the poor statistics resulting from the few HBs that exist for $T <$

TABLE 1 Parameters obtained from Arrhenius analysis of rate constants obtained for HB dynamics according to Eq. 2

HB type	Symbol	T-Range K	A ps^{-1}	$E^{\ddagger}$ kJ mol^{-1}	$\tilde{A}$ ps^{-1}	$\tilde{E}^{\ddagger}$ kJ mol^{-1}
Water (bulk)-water (bulk)	*w*	280–390	10	7	1	5
Water (side-group chain)-water (side-group chain)	*sc*	280–390	9	7	—	—
Water (bulk)-water (surf.)	*sw*	280–390	15	7	—	—
Peptide-water (surf.)	*ps*	280–320	60	12	17	10
Peptide-water (surf.)	*ps*	320–390	2	4	0.2	≈0
Peptide-peptide	*pp*	280–320	30	8	—	—
Peptide-peptide	*pp*	330–390	4	6	—	—

320 K, and the relatively poor convergence for long-time decay, only allow for a partial analysis. Nonetheless, we are able to make several important observations. First, the short-time regime $t < 4$ ps can be used to obtain an approximation to k_{pp} in a similar fashion as above (see Fig. 9). Below 330 K, k_{pp} may be interpreted as having approximately Arrhenius behavior with $E^{\ddagger}_{pp} \approx 8\,\mathrm{kJ/mol}$ (see Fig. 9 *c*). This barrier is similar to that for HBs between bulk water but less than those between the peptide and solvent waters (see Table 1 for a detailed comparison). Above 330 K, where a larger number of peptide/peptide HBs improves the statistics of $c_{pp}(t)$, k_{pp} is again found to have an approximate Arrhenius behavior. At these temperatures the peptide/peptide HBs exhibit a slightly lower activation barrier for breaking of $E^{\ddagger}_{pp} \approx 6\,\mathrm{kJ/mol}$, which is larger than that for peptide/water HBs in the same temperature regime, and will thus stabilize the folded state. The increase of thermal energy, which allows peptide/water HBs to break more easily, decreases the stability of the open state but has less effect on the folded state, which is in part stabilized by peptide/peptide HBs. Second, although the long-time decay of the function has too much numerical noise to provide a reliable fitting it is evident that the probability to recover the same HB pair decreases rapidly with increasing temperature above 330 K (see Fig. 7 *d*). This is in accord with the above observation of a speedup of the peptide's backbone motion in this same temperature regime. Increasing fluctuations of the peptide backbone above 330 K result in breaking peptide/peptide bonds more rapidly and decreasing the probability with which they reform. This effect will counter the stabilization from peptide/peptide HBs for the folded state, and will eventually lead to the unfolding at higher temperature.

CONCLUSIONS

The presented study is successfully able to reproduce the inverse temperature transition of a minimal elastin model at ~40–60°C. Additionally, an unfolding transition is identified at temperatures approaching the normal boiling point of water. Our simulations reproduce the key observations obtained from FT-IR, CD, DSC, and PPC experiments in the companion study (Nicolini et al., 2004) of the same water-solvated octapeptide. Due to the small size of the system two broad temperature regimes are found both in experiment and in the simulations: the ITT regime (at ~10–60°C) and the unfolding regime at $\sim T > 60$°C, where the structure has a maximum probability of being folded at $T \approx 60$°C. A detailed molecular picture involving a reaction coordinate and a free energy profile for this process is presented along with a thorough time-correlation function analysis of the hydrogen-bond dynamics and kinetics within the peptide as well as at the peptide/water interface. In particular, the two regimes are characterized by changes in a dynamical two-state equilibrium between open and closed conformations and a change of the HB dynamics involving interfacial water molecules.

In a nutshell, our data suggest a simple qualitative picture of the observed transitions. At low temperatures, a relatively strong peptide/water interaction stabilizes open conformations relative to closed ones. The increase of thermal energy decreases the stability of the extended state but has less effect on the folded conformation, which is in part stabilized by peptide/peptide HBs. Thus, there is a shift in equilibrium and one observes an increase in folded structures and hence the ITT. A second important contributing factor is the increase of peptide backbone fluctuations above the ITT and the resulting entropic stability. However, the large librational amplitude motion of the peptide backbone can provide sufficient thermal excitation to break these peptide/peptide HBs at higher temperatures, which ultimately leads to a second, unfolding, transition.

The current work, based upon a temperature scan using 32-ns simulations of an octapeptide, gives further support to the conclusions of previous studies employing much shorter MD simulations on longer poly(VPGVG) peptides (Li et al., 2001a,b, 2002; Li and Daggett, 2002). As in these studies, we also observe a decrease in the peptide/water interactions around the ITT and a speedup of the peptide backbone dynamics above this transition. Although our longer simulation times do qualitatively agree with the findings of this earlier work the present study is able to provide a more quantitative analysis of the dynamical processes associated with the peptide structural transitions. Novel findings related to the interrelation of peptide/water HB dynamics and peptide librational entropy, which are complementary aspects of the ITT and unfolding transitions as opposed to being alternate

models, are only possible due to these quite-long MD trajectories. Thus, the current work emphasizes the importance of detailed statistical-mechanical analysis in constructing atomic-level pictures of complex biomolecular processes.

The limitation of the current approach, however, is that it is not clear at present how all of the factors, which have been isolated as key ingredients in the peptide structural transitions, will apply to large polypeptides. Although it is highly likely that decrease in peptide/water HB interactions and peptide librational entropy will remain important ingredients, the relative weights of the two factors in larger polymers is unknown. Most notably, entropy contributions from changes in the solvation shell around the hydrophobic side chains may become an important factor for larger systems where the solvent-accessible surface is dominated by hydrophobic contacts to a greater extent than for the current octapeptide. Also, the energetic/entropic contribution of bridging waters in larger polymers where the folded peptide may be truly said to have an ''inside'' is currently an open issue. To address these questions, future combined experimental and theoretical work on $GVG(VPGVG)_n$ with $n = 2$ and 3 including mutant structures as well as tropoelastins is currently underway.

This work has benefited immensely from insightful and enjoyable interactions with Amalendu Chandra, Alfons Geiger, Helmut Grubmüller, Matthias Müller, Chiara Nicolini, Nikolaj Otte, Hermann Weingärtner, Roland Winter, and Xiao-Ying Yu.

The simulations were carried out at Bovilab at Ruhr-Universität Bochum, and we thank Deutsche Forschungsgemeinschaft (FOR 436) and Fonds der Chemischen Industrie for partial financial support.

REFERENCES

Aalten, D. V., B. D. Groot, J. Findlay, H. Berendsen, and A. Amadei. 1997. A comparison of techniques for calculating protein essential dynamics. *J. Comp. Chem.* 18:169–181.

Aaron, B., and J. Gosline. 1980. Optical properties of single elastin fibres indicate random protein conformation. *Nature.* 287:865–867.

Amadei, A., A. Linssen, and H. Berendsen. 1993. Essential dynamics of proteins. *Proteins Struct. Funct. Gen.* 17:412–425.

Andriciolaei, I., and M. Karplus. 2001. On the calculation of entropy from covariance matrices of the atomic fluctuations. *J. Chem. Phys.* 115:6289–6292.

Arad, M. G. O. 1990. Depsipeptide analogues of elastin repeating sequences: conformational analysis. *Biopolymers.* 29:1651–1668.

Balsera, M., W. Wriggers, Y. Oono, and K. Schulten. 1996. Principal component analysis and long time protein dynamics. *J. Phys. Chem.* 100:2567–2572.

Brooks III, C., and M. Karplus. 1983. Deformable stochastic boundaries in molecular dynamics. *J. Chem. Phys.* 79:6312–6325.

Chandra, A. 2000. Effects of ion atmosphere on hydrogen-bond dynamics in aqueous electrolyte solutions. *Phys. Rev. Lett.* 85:768–771.

Cook, W., H. Einspahr, T. Trapane, D. Urry, and C. Bugg. 1980. Crystal structure and conformation of the cyclic trimer of a repeat pentapeptide of elastin, cyclo-(*l*-valyl-*l*-prolylglycyl-*l*-valylglycyl)$_3$. *J. Am. Chem. Soc.* 102:5502–5505.

Debelle, L., and A. Alix. 1999. The structures of elastins and their function. *Biochimie.* 81:981–994.

Debelle, L., A. Alix, M. Jacob, J. Huvenne, M. Berjot, B. Sombret, and P. Legrand. 1995. Bovine elastin and kappa-elastin secondary structure determination by optical spectroscopies. *J. Biol. Chem.* 270:26099–26103.

Debelle, L., and A. Tamburro. 1999. Elastin: molecular description and function. *Int. J. Biochem. Cell Biol.* 31:261–272.

Dixit, S., J. Crain, W. Poon, J. Finney, and A. Soper. 2002. Molecular segregation observed in a concentrated alcohol-water solution. *Nature.* 416:829–832.

Eichinger, M., H. Grubmüller, H. Heller, and P. Tavan. 1997. FAMUSAMM: an algorithm for rapid evaluation of electrostatic interactions in molecular dynamics simulations. *J. Comp. Chem.* 18:1729–1749.

Eichinger, M., H. Heller, and H. Grubmüller. 2000. EGO—an efficient molecular dynamics program and its application to protein dynamics simulations. *In* Molecular Dynamics on Parallel Computers. R. Esser, P. Grassberger, J. Grotendorst, and M. Lewerenz, editors. World Scientific, Singapore. 154–174.

Fleming, W., C. Sullivan, and D. Torchia. 1980. Characterization of molecular motions in ^{13}C-labeled aortic elastin by ^{13}C-^{1}H magnetic double resonance. *Biopolymers.* 19:597–617.

García, A. E. 1992. Large-amplitude nonlinear motions in proteins. *Phys. Rev. Lett.* 68:2696–2699.

Hoeve, C., and P. Flory. 1974. The elastic properties of elastin. *Biopolymers.* 13:677–686.

Hyvärinen, A., J. Karhunen, and E. Oja. 2001. Independent Component Analysis. John Wiley & Sons. Chapt. 6.

Jorgensen, W., J. Chandrasekhar, J. Madura, R. Impey, and M. Klein. 1983. Comparison of simple potential functions for simulating liquid water. *J. Chem. Phys.* 79:926–935.

Kurková, D., J. Kříž, P. Schmidt, J. Dybal, J. Rodriguez-Cabello, and M. Alonso. 2003. Structure and dynamics of two elastin-like polypentapeptides studied by NMR spectroscopy. *Biomacromolecules.* 4:589–601.

Li, B., D. Alonso, B. Bennion, and V. Daggett. 2001a. Hydrophobic hydration is an important source of elasticity in elastin-based biopolymers. *J. Am. Chem. Soc.* 123:11991–11198.

Li, B., D. Alonso, and V. Daggett. 2001b. The molecular basis for the inverse temperature transition of elastin. *J. Mol. Biol.* 305:581–592.

Li, B., D. Alonso, and V. Daggett. 2002. Stabilization of globular proteins via introduction of temperature-activated elastin-based switches. *Structure.* 10:989–998.

Li, B., and V. Daggett. 2002. Molecular basis for the extensibility of elastin. *J. Musc. Res. Cell Motil.* 23:561–573.

Luzar, A. 2000. Extent of inter-hydrogen bond correlations in water. Temperature effect. *Chem. Phys.* 258:267–276.

Luzar, A., and D. Chandler. 1996a. Effect of environment on hydrogen bond dynamics in liquid water. *Phys. Rev. Lett.* 76:928–931.

Luzar, A., and D. Chandler. 1996b. Hydrogen bond kinetics in liquid water. *Nature.* 379:55–57.

MacKerell, A. D., D. Bashford, M. Bellott, R. L. Dunbrack, J. D. Evanseck, M. J. Field, S. Fischer, J. Gao, H. Guo, S. Ha, D. Joseph-McCarthy, L. Kucinir, K. Kuczera, F. T. K. Lau, C. Mattos, S. Michnick, T. Ngo, D. T. Nguyen, B. Prodhom, W. E. Reiher, B. Roux, M. Schlenkrich, J. C. Smith, R. Stote, J. Straub, M. Watanabe, J. Wiorkiewicz-Kuczera, D. Yin, and M. Karplus. 1998. All-atom empirical potential for molecular modeling and dynamics studies of proteins. *J. Phys. Chem. B.* 102:3586–3617.

Martino, M., T. Perri, and A. Tamburro. 2002. Biopolymers and biomaterials based on elastomeric proteins. *Mol. Biosci.* 2:319–328.

McLachlan, A. D. 1979. Gene duplications in the structural evolution of chymotrypsin. *J. Mol. Biol.* 128:49–77.

Nath, N., and A. Chilkoti. 2001. Interfacial phase transition of an environmentally responsive elastin biopolymer adsorbed on functionalized gold nanoparticles studied by colloidal surface plasmon resonance. *J. Am. Chem. Soc.* 123:8197–8202.

Nicolini, C., R. Ravindra, B. Ludolph, and R. Winter. 2004. Characterization of the temperature- and pressure-induced inverse and reentrant

transition of the minimum elastin-like polypeptide GVG(VPGVG) by DSC, PPC, CD, and FT-IR spectroscopy. *Biophys. J.* 86:1385–1392.

Omta, A. W., M. F. Kropman, S. Woutersen, and H. J. Bakker. 2003. Negligible effect of ions on the hydrogen-bond structure in liquid water. *Science.* 301:347–349.

Partridge, S. 1962. Elastin. *Adv. Protein Chem.* 17:227–302.

Pasquali-Ronchetti, I., C. Fornieri, M. Baccarani-Contri, and D. Quaglino. 1995. Ultrastructure of elastin. *In* The Molecular Biology and Pathology of Elastic Tissues. CIBA Foundation, John Wiley & Sons Ltd. 31–42.

Perry, A., M. Stypa, J. Foster, and K. Kumashiro. 2002. Observation of the glycines in elastin using ^{13}C and ^{15}N solid-state NMR spectroscopy and isotopic labeling. *J. Am. Chem. Soc.* 124:6832–6833.

Pratt, L., and A. Pohorille. 2002. Hydrophobic effects and modeling of biophysical aqueous solution interfaces. *Chem. Rev.* 102:2671–2691.

Reiersen, H., A. Clarke, and A. Rees. 1998. Short elastin-like peptides exhibit the same temperature-induced structural transitions as elastin polymers: implications for protein engineering. *J. Mol. Biol.* 283:255–264.

Reiersen, H., and A. Rees. 2001. The hunchback and its neighbours: proline as an environmental modulator. *Trends Biochem. Sci.* 26:679–684.

Savitzky, A., and M. Golay. 1964. Smoothing and differentiation of data by simplified least squares procedures. *Anal. Chem.* 36:1627–1639.

Schlitter, J. 1993. Estimation of absolute and relative entropies of macromolecules using the covariance matrix. *Chem. Phys. Lett.* 215:617–621.

Starr, F., J. Nielsen, and H. Stanley. 1999. Fast and slow dynamics of hydrogen bonds in liquid water. *Phys. Rev. Lett.* 82:2294–2297.

Stillinger, F. H. 1975. Theory and molecular models for water. *Adv. Chem. Phys.* 31:1–101.

Tamura, T., T. Yamaoka, A. Panitch, and D. Tirrell. 2000. Effects of temperature and pressure on the aggregation properties of an engineered elastin model polypeptide in aqueous solution. *Biomacromolecules.* 1:552–555.

Tarek, M., and D. Tobias. 1999. Environment dependence of the dynamics of protein hydration water. *J. Am. Chem. Soc.* 121:9740–9741.

Tarek, M., and D. Tobias. 2002a. Role of protein-water hydrogen bond dynamics in the protein dynamical transition. *Phys. Rev. Lett.* 88:1381011–1381014.

Tarek, M., and D. Tobias. 2002b. Single-particle and collective dynamics of protein hydration water: a molecular dynamics study. *Phys. Rev. Lett.* 89:2755011–2755014.

Torchia, D., and K. Piez. 1973. Mobility of elastin chains as determined by ^{13}C nuclear magnetic resonance. *J. Mol. Biol.* 76:419–424.

Urry, D. 1993. Molecular machines: how motion and other functions of living organisms can result from reversible chemical changes. *Angew. Chemie Int. Ed. (Engl.).* 32:819–841.

Urry, D. 1997. Physical chemistry of biological free energy transduction as demonstrated by elastic protein-based polymers. *J. Phys. Chem. B.* 101:11007–11028.

Urry, D., T. Hugel, M. Seitz, H. Gaub, L. Sheiba, J. Dea, J. Xu, and T. Parker. 2002. Elastin: a representative ideal protein elastomer. *Phil. Trans. R. Soc. Lond. B.* 357:169–184.

Urry, D., M. Long, and H. Sugano. 1978. Cyclic analog of elastin polyhexapeptide exhibits an inverse temperature transition leading to crystallization. *J. Biol. Chem.* 253:6301–6302.

Urry, D., R. Shaw, and K. Prasad. 1985a. Polypentapeptide of elastin: temperature dependence of ellipticity and correlation with elastomeric force. *Biochem. Biophys. Res. Commun.* 130:50–57.

Urry, D., T. Trapane, M. Iqbal, C. Venkatachalam, and K. Prasad. 1985b. Carbon-13 NMR relaxation studies demonstrate an inverse temperature transition in the elastin polypentapeptide. *Biochimie.* 24:5182–5189.

Urry, D., T. Trapane, M. Long, and K. Prasad. 1983. Test of the librational entropy mechanism of elasticity of polypentapeptide of elastin. *J. Chem. Soc. Faraday Trans. 1.* 79:853–868.

van der Spoel, D., P. van Maaren, and J. Berendsen. 1998. A systematic study of water models for molecular simulation: derivation of water models optimized for use with a reaction field. *J. Chem. Phys.* 108: 10220–10230.

Wasserman, Z., and F. Salemme. 1990. A molecular dynamics investigation of the elastomeric restoring force in elastin. *Biopolymers.* 29:1613–1631.

Xu, H., and B. Berne. 2001. Hydrogen-bond kinetics in the solvation shell of a polypeptide. *J. Phys. Chem. B.* 105:11929–11932.